Structural Eng./Earthquake Eng. Vol. 10, No. 2, 71s—82s, July 1993
Japan Society of Civil Engineers (J. Struct. Mech. Earthquake Eng. No. 471/I—24)

MULTI-MODE FLUTTER ANALYSIS AND TWO & THREE DIMENSIONAL MODEL TESTS ON BRIDGES WITH NON-ANALOGOUS MODAL SHAPES

Hiroshi TANAKA*, Nobumichi YAMAMURA**
and Naruhito SHIRAISHI***

Coupled flutter of non-analogous vertical and torsional modes, which may typically occur in mono-cable suspension or single plane cable-stayed bridges, for example, and multi-mode flutter including higher modes are studied both analytically and experimentally. In such cases, the lateral locations of rotational center of girder vary along the span, so that a two-dimensional or spring mounted model test loses its validity. The proposed multi-mode flutter analysis using the flutter derivatives is expected to be useful to predict the coupled non-analogous and/or multi-mode flutter along with the three-dimensional model tests.

Key Words: *coupled flutter, flutter derivatives, complex eigen value analysis*

1. INTRODUCTION

Evaluation of aerodynamic stability is one of the most important aspects in the design of long span suspended bridges (e.g., suspension and cable-stayed bridge etc.). Recently these bridges have become more susceptible to a variety of wind-induced instabilities due to the construction trend to build them large, slender and flexible. Above all, flutter phenomena are disastrous as shown by the well known collapse of the original Tacoma Narrows Bridge in 1940. After the accident, wind tunnel tests have become indispensable procedure to ensure the safety for the design of long span suspension bridges[1]. The first choice for this purpose is the section model test wherein a rigid scaled model of a typical bridge section is spring-mounted and is tested under laminar or turbulent flows. The method has prevailed for its simplicity and economy. However, the section model tests can be a possible choice to represent the prototype bridge action only when all of the following conditions are fulfilled for the prototype bridges:

(1) Aerodynamic characteristics of girder do not vary along the span.
(2) Modal shapes of vertical bending and torsional oscillations are analogous in the coupled flutter.
(3) Higher modes do not virtually participate in the coupled flutter.
(4) Aerodynamic damping due to the lateral motion of girder, the motions of cables and towers is insignificant.

Three-dimensional (i.e., full-bridge) models are used when these conditions are not realized. However, even the full-bridge models, which are expensive both in models and wind tunnel facilities, are not necessarily capable of satisfying simultaneously all the similarity requirements of prototype bridges.

The third approach is the analytical methods which have been advanced by Bleich[2], Scanlan[3] etc. and recently by Miyata & Yamada[4] incorporating the self-excited forces (under laminar flows) in equation of motion. Bleich who also discussed the coupling of non-analogous modes and Scanlan applied the self-excited forces only on girder, thus they disregarded the additional damping effects by the motion of cables and towers. Miyata & Yamada included them, but the analysis is based on the Theodorsen's aerodynamic forces on flat plates and is not generalized for bluff body structures.

The present paper intends to extend the analytical approach. First, it provides a complex eigenvalue and vector solutions for multi-mode flutter of space-frame structures using the flutter derivatives[3),5]. To formulate possible coupling between lateral and other (vertical or torsional) motions of girder, newly defined flutter

* Member of JSCE, Dr. Eng., Bridge Engineer, Bridge Design Dept., Hitachi Zosen Corp. (1-3-40, Sakurajima, Konohana-ku, Osaka 554)

** Member of JSCE, Dr. Eng., Technical Supervisor, Bridge Design Dept., Hitachi Zosen Corp.

*** Member of JSCE, Dr. Eng., Professor, Dept. of Civil Engineering, Kyoto University

derivatives $P^*_0 \cdot H^*_0 \cdot A^*_0$ are introduced. The flutter derivatives are applied to all members including girder, cables and towers as the variable for each member. The present method may be useful in such cases as; (1) the eigenmodes of bending and torsional oscillations are not analogous; (2) higher modes participate in the coupled flutter (i.e., multi-mode flutter); (3) the lateral motion of girder, the motions of cables and towers provide significant aerodynamic effects; (4) aerodynamic characteristics of girder including the flutter derivatives vary along the span.

The paper proceeds to an example of mono-cable suspension bridge with center-span of 450m, where the flutter behavior is examined by the present analysis as well as by two- and three-dimensional model tests.

2. SELF-EXCITED FORCES AND DYNAMIC EQUATIONS

Extension of Scanlan's formulation[3),5)] leads to dynamic equations in matrix form by the displacement method[6),7),8)]. First, the equations of motion are expressed as (see **Fig.1** for notation),

$$[M]\cdot\{\ddot{U}_i(t)\}+[C]\cdot\{\dot{U}_i(t)\}+[K]\cdot\{U_i(t)\}=\{F_i(t)\} \quad \cdots\cdots (1)$$

where [M] is the mass matrix, [C] is the structural damping matrix, [K] is the stiffness matrix, $\{U_i(t)\} = \{x_i(t), y_i(t), z_i(t), \alpha_i(t), \beta_i(t), \theta_i(t)\}$ is the displacement vector of a member (i), and $\{F_i(t)\}$ is the wind load vector (= self-excited force). The displacement vector, $\{U_i(t)\}$ is expressed by eigenmode functions $\{\phi_{im}\}$ and generalized coordinates $X_m(t)$, where m=1,2,···, M and M is the number of modes, as follows:

$$\left.\begin{aligned}\{U_i(t)\} &= \sum_{m=1}^{M}\{\phi_{im}\}\cdot X_m(t)\\ \phi_{im} &= (\phi_{km}+\phi_{lm})/2 \ \text{(Mode shape at the center of i - th member)}\end{aligned}\right\} \quad \cdots\cdots (2)$$

Pre-multiplying Eq.(1) by $\{\phi_{im}\}^T$, it becomes

$$\left.\begin{aligned}&\ddot{X}_m(t)+2h^s_m\cdot\omega_m\cdot\dot{X}_m(t)+\omega_m^2\cdot X_m(t)\\ &\quad=\{\phi_{im}\}^T\cdot\{F_i(t)\}/M^*_m\\ &M^*_m=\{\phi_{im}\}^T\cdot[M]\cdot\{\phi_{im}\}\end{aligned}\right\} \quad \cdots\cdots (3)$$

where h^s_m and ω_m are, respectively, the structural damping ratio in still air and circular frequency [rad/s] of the m-th mode. Under the assumption that the girder is regarded as horizontal and the wind acts on bridge laterally at right angle, the components of wind vector

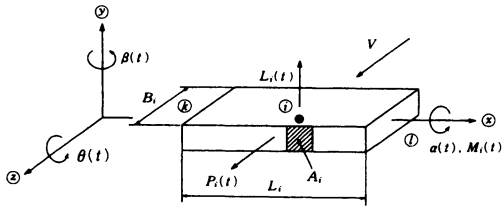

Fig.1 Member ⓘ in global coordinate

$\{F_i(t)\}$ in Eq.(3) can be expressed as

$$F_i(t) = \{\, 0, L_i(t), P_i(t), M_i(t), 0, 0 \,\} \quad \cdots\cdots (4)$$

$$\left.\begin{aligned}P_i(t) &= (\rho\cdot V_i^2/2)\cdot A_i\cdot K_i\cdot[P^*_{0i}, P^*_{1i},\\ &\quad P^*_{2i}, P^*_{3i}]\cdot\{\dot{y}_i(t)/V_i, \dot{z}_i(t)/V_i,\\ &\quad B_i\cdot\dot{\alpha}_i(t)/V_i, K_i\cdot\alpha_i(t)\}\cdot L_i\\ L_i(t) &= (\rho\cdot V_i^2/2)\cdot B_i\cdot K_i\cdot[H^*_{0i}, H^*_{1i},\\ &\quad H^*_{2i}, H^*_{3i}]\cdot\{\dot{z}_i(t)/V_i, \dot{y}_i(t)/V_i,\\ &\quad B_i\cdot\dot{\alpha}_i(t)/V_i, K_i\cdot\alpha_i(t)\}\cdot L_i\\ M_i(t) &= (\rho\cdot V_i^2/2)\cdot B_i^2\cdot K_i\cdot[A^*_{0i}, A^*_{1i},\\ &\quad A^*_{2i}, A^*_{3i}]\cdot\{\dot{z}_i(t)/V_i, \dot{y}_i(t)/V_i,\\ &\quad B_i\cdot\dot{\alpha}_i(t)/V_i, K_i\cdot\alpha_i(t)\}\cdot L_i\end{aligned}\right\} \cdot (5)$$

$K_i = B_i\cdot\omega/V_i \fallingdotseq B_i\cdot\omega_R/V_i$: the reduced flutter frequency [see Eq. (14)]

$$\left.\begin{aligned}&P^*_{0i} = -(dC_D/d\alpha)/K_i = -C'_{Di}/K_i\\ &P^*_{1i} = -2C_{Di}/K_i,\ P^*_{2i} \fallingdotseq 0^{3)}\\ &P^*_{3i} = (dC_{Di}/d\alpha)/K_i^2 = C'_{Di}/K_i^2\\ &H^*_{0i} \fallingdotseq -2C_{Li}/K_i,\ A^*_{0i} = -2C_{Mi}/K_i\end{aligned}\right\} \quad \cdots\cdots (6)$$

where $P_i(t)$, $L_i(t)$, $M_i(t)$ are, respectively, the drag force, lift force and moment. ρ is the air density [$t\cdot s^2/m^4$], V_i is the wind velocity [m/s], A_i is the area (per unit span) subjected to wind [m^2/m], B_i is the lateral girder width [m], L_i is the member length [m], C_{Di} is the drag coefficient defined for A_i, ω is the flutter circular frequency [rad/s], $P^*_{ji}(K_i)\cdot H^*_{ji}(K_i)\cdot A^*_{ji}(K_i)$ are dimensionless flutter derivatives of i-th member. All derivatives are double of those given by Scanlan[3)] and $H^*_{2i}(K_i)\cdot H^*_{3i}(K_i)\cdot A^*_{1i}(K_i)$ have opposite sign due to upward y-axis adopted here.

Note that the flutter derivatives of Eq. (6) are derived with the quasi-steady theory, of which P^*_{ji} (j=1,2,3) advanced by Scanlan[3),5)] have found some applications[6),7),11)] and their validity seems to be confirmed. However, $P^*_{0i}\cdot H^*_{0i}\cdot A^*_{0i}$ are tentatively introduced by the authors to include possible coupling between lateral and other (vertical or torsional) motions

in the flutter analysis, so their effects and validity are yet to be proved.

The eigenmode function $\{\phi_{im}\}$ is defined as follows:

$$\{\phi_{im}\}=\{\phi^{x}_{im}, \phi^{y}_{im}, \phi^{z}_{im}, \phi^{\alpha}_{im}, \phi^{\beta}_{im}, \phi^{\theta}_{im}\} \quad \cdots\cdots (7)$$

The self-excitation terms for girder are derived by inserting Eqs. (2), (4), (5) and (7) into Eq. (3) :

$$\{\phi_{im}\}^T \cdot \{F_i(t)\} / M^*_m = [\{\phi^z_{im}\}^T \cdot \{P_i(t)\} + \{\phi^y_{im}\}^T \{L_i(t)\} + \{\phi^{\alpha}_{im}\}^T \cdot \{M_i(t)\}] / M^*_m \quad \cdots\cdots (8)$$

$$\left.\begin{aligned}
&\{\phi^z_{im}\}^T \cdot \{P_i(t)\} = (\rho/2)\cdot\omega\cdot\sum_i A_i \cdot B_i \cdot \\
&\quad \phi^z_{im}\cdot[P^*_{0i}, P^*_{1i}, P^*_{2i}, P^*_{3i}]\cdot \\
&\quad \left\{\sum_n \dot{X}_n(t)\cdot\phi^y_{in}, \sum_n \dot{X}_n(t)\cdot\phi^z_{in}, B_i\cdot \right. \\
&\quad \left. \sum_n \dot{X}_n(t)\cdot\phi^{\alpha}_{in}, B_i\cdot\omega\cdot\sum_n X_n(t)\cdot\phi^{\alpha}_{in}\right\}\cdot L_i \\
&\{\phi^y_{im}\}^T \cdot \{L_i(t)\} = (\rho/2)\cdot\omega\cdot\sum_i B_i^2 \cdot \\
&\quad \phi^y_{im}\cdot[H^*_{0i}, H^*_{1i}, H^*_{2i}, H^*_{3i}]\cdot \\
&\quad \left\{\sum_n \dot{X}_n(t)\cdot\phi^z_{in}, \sum_n \dot{X}_n(t)\cdot\phi^y_{in}, B_i\cdot \right. \\
&\quad \left. \sum_n \dot{X}_n(t)\cdot\phi^{\alpha}_{in}, B_i\cdot\omega\cdot\sum_n X_n(t)\cdot\phi^{\alpha}_{in}\right\}\cdot L_i \\
&\{\phi^{\alpha}_{im}\}^T \cdot \{M_i(t)\} = (\rho/2)\cdot\omega\cdot\sum_i B_i^3 \cdot \\
&\quad \phi^{\alpha}_{im}\cdot[A^*_{0i}, A^*_{1i}, A^*_{2i}, A^*_{3i}]\cdot \\
&\quad \left\{\sum_n \dot{X}_n(t)\cdot\phi^z_{in}, \sum_n \dot{X}_n(t)\cdot\phi^y_{in}, B_i\cdot \right. \\
&\quad \left. \sum_n \dot{X}_n(t)\cdot\phi^{\alpha}_{in}, B_i\cdot\omega\cdot\sum_n X_n(t)\cdot\phi^{\alpha}_{in}\right\}\cdot L_i
\end{aligned}\right\} \quad (9)$$

For main cable of suspension bridges, only the $P^*_{1i}(K_i)$ and $H^*_{1i}(K_i)$ terms in Eq. (9) are necessary, and for $H^*_{1i}(K_i)$ the quasi-steady formula may be applied, yielding:

$$H^*_{1i}(K_i) = -C_{Di}/K_i = -(1/2\pi)\cdot C_{Di}\cdot V_i/(f\cdot B_i) \quad \cdots\cdots (10)$$

where f is the flutter frequency [Hz] and B_i is the diameter of the cable [m]. For the tower members, only the P^*_{1i} term in Eq. (9) is necessary and L_i in Eq. (9) should refer to the vertical length of the members. The hanger member area subjected to the wind pressure should be included in the main cable and the girder area, weighted by the ratio of the drag coefficient of hanger to main cable or girder, respectively.

Then, a set of coupled flutter equations is obtained by inserting Eq. (9) into Eq. (3).

$$\ddot{X}_m(t) + 2h^s_m\cdot(\omega_m/\omega)\cdot\omega\cdot\dot{X}_m(t) + \omega_m^2\cdot X_m(t) = \sum_n E_{mn}\cdot\omega\cdot\dot{X}_n(t) + \sum_n F_{mn}\cdot\omega^2\cdot X_n(t) \quad \cdots\cdots (11)$$

$$\left.\begin{aligned}
&E_{mn} = (\rho/2M^*_m)\cdot\sum_i B_i\cdot\{\phi^y_{im},\phi^z_{im},\phi^{\alpha}_{im}\}^T\cdot[H]\cdot \\
&\quad \{\phi^y_{in},\phi^z_{in},\phi^{\alpha}_{in}\}\cdot L_i \\
&[H] = \begin{bmatrix} H^*_{1i}(K_i)\cdot B_i & H^*_{0i}(K_i)\cdot B_i & H^*_{2i}(K_i)\cdot B_i^2 \\ P^*_{0i}(K_i)\cdot A_i & P^*_{1i}(K_i)\cdot A_i & P^*_{2i}(K_i)\cdot A_i\cdot B_i \\ A^*_{1i}(K_i)\cdot B_i^2 & A^*_{0i}(K_i)\cdot B_i^2 & A^*_{2i}(K_i)\cdot B_i^3 \end{bmatrix}
\end{aligned}\right\} \quad (12)$$

$$F_{mn} = (\rho/2M^*_m)\cdot\sum_i B_i^2\cdot\{\phi^y_{im},\phi^z_{im},\phi^{\alpha}_{im}\}^T\cdot \{H^*_{3i}(K_i)\cdot B_i, P^*_{3i}(K_i)\cdot A_i, A^*_{3i}(K_i)\cdot B_i^2\}\cdot\phi^{\alpha}_{in}\cdot L_i \quad \cdots\cdots (13)$$

3. COMPLEX EIGENVALUE EQUATIONS

The complex generalized coordinates $X_m(t)$, associated with the complex flutter circular frequency ω, are introduced as follows:

$$\left.\begin{aligned}
&X_m(t) = X_{m0}\cdot e^{i\omega t},\ X_{m0} = X^R_{m0} + i\cdot X^I_{m0} \\
&\omega = \omega_R + i\cdot\omega_I = (1 + i\cdot h)\cdot\omega_R
\end{aligned}\right\} \quad (14)$$

$$\left.\begin{aligned}
&\left[(X^R_{m0})^2 + (X^I_{m0})^2\right]^{1/2} : \text{the amplitude of the } m\text{-th mode } (=|X_{m0}|) \\
&\theta_m = \tan^{-1}(X^I_{m0}/X^R_{m0}) : \text{the phase-shift of the } m\text{-th mode (rad)}
\end{aligned}\right\} \quad \cdots\cdots (15)$$

where ω_R is the flutter circular frequency [rad/s] and $h = \omega_I/\omega_R$ ($= \delta/2\pi$) is the sum of structural and aerodynamic damping.

The complex eigenvalue equations, derived from inserting $X_m(t)$ of Eq.(14) into Eq.(11), are as follows.

$$([G_{mn}]-[\lambda])\cdot\{X_{m0}\} = \begin{bmatrix} G_{11}-\lambda & G_{12}\cdots & G_{1m} \\ G_{21} & G_{22}-\lambda & G_{2m} \\ \cdot & \cdot & \cdot \\ \cdot & \cdot & \cdot \\ G_{m1} & G_{m2}\cdots & G_{mm}-\lambda \end{bmatrix}\cdot\begin{Bmatrix} X_{10} \\ X_{20} \\ \cdot \\ \cdot \\ X_{m0} \end{Bmatrix} = 0 \quad \cdots (16)$$

$$\left.\begin{aligned}
&G_{mm} = [F_{mm} + 1 + i\cdot\{E_{mm} - 2h^s_m\cdot(\omega_m/\omega)\}]/\omega_m^2 \\
&G_{mn} = (F_{mn} + i\cdot E_{mn})/\omega_m^2 (m \neq n) \\
&[\lambda] = \text{Diag}\,[1/\omega^2]\ (\text{Diag. matrix})
\end{aligned}\right\} \quad \cdots\cdots (17)$$

For a set of eigenvectors $\{X_{m0}\}$ to have solution:

$$\det([G_{mn}] - [\lambda]) = \det([G_{mn}] - \mathrm{Diag}[1/\omega^2]) = 0 \quad \cdots\cdots (18)$$

Eq. (18) contains the complex unknown ω, then arbitrary initial values (e.g., $\omega_m/\omega = 1$) may be given (the choice of ω_m is briefed below) and ω and $\{X_{m0}\}$ can be determined with iterative calculations of Eqs.(17) and (18). The following convergence criteria is appropriate with ε - value of 10^{-3}~10^{-4} (k: number of iterations).

$$|\omega_k - \omega_{k-1}| / |\omega_k| < \varepsilon \quad \cdots\cdots (19)$$

Once ω is determined, logarithmic damping $\delta = 2\pi \cdot \omega_I/\omega_R$ may be plotted against wind velocity $V = B \cdot \omega_R / K_0$ for a typical member, where K_0 is an arbitrarily given reduced frequency.

When the rank of the matrix in Eq.(16) is M, M-set of flutter frequencies ω_n and a matrix of eigenvectors $\{X^0_{mn}\}$(n = 1,2,..., M) will be obtained. It should be noted, however, that the calculations of Eqs.(18) and (19) need not necessarily be carried out for all modes. One can easily find the flutter frequency ω_n and amplitude $|X^0_{mn}|$ in which the m-th (e.g., torsional) mode is dominant with the following Eq. (20):

$$|X^0_{mn}|_{max} = \mathrm{MAX}\left[|X^0_{m1}|, |X^0_{m2}|, \cdots, |X^0_{mM}|\right] \quad \cdots\cdots (20)$$

However, if the choice of the critical modal combination is difficult, the comparison of V-δ curve for ω_n and $\{X^0_{mn}\}$ (n=1,2,..,M) may be convenient.

Through the above procedure for a series of arbitrarily chosen values of $K_{0j} = B_0 \cdot \omega_m / V_{0j}$ for a typical member, the most critical V-δ curve can be found, then the flutter velocity V_{cr} is given as its zero-crossing point.

4. SINGLE DEGREE OF FREEDOM FLUTTER

Galloping and stall flutter are the typical single mode flutter. For these cases, flutter frequency and critical velocity can be derived from Eq. (16) using its simplified form:

$$\lambda = G_{11} = \left[F_{11} + 1 + i \cdot \{E_{11} - 2h^s_1 \cdot (\omega_1/\omega)\}\right] / \omega_1^2 \quad \cdots\cdots (21)$$

The further simplified cases of single degree of freedom (SDOF) flutter, which correspond to section model behavior, are summarily discussed here.

(1) Galloping

The component of eigenmode function $\{\phi^x_{im}, \phi^y_{im}, \phi^z_{im}, \phi^\alpha_{im}, \phi^\beta_{im}, \phi^\theta_{im},\}$ is reduced to {0, 1, 0, 0, 0, 0}. Then $F_{11} = 0$ ($\because \phi^\alpha_{im} = 0$) and E_{11} is rewritten as follows ($\omega_1 \fallingdotseq \omega$):

$$E_{11} = \rho \cdot B^2 \cdot L \cdot H^*_1 / (2M^*) = \rho \cdot B^2 \cdot H^*_1 / (2m) \quad \cdots\cdots (22)$$

where m is mass per unit length $[t \cdot s^2 / m^2]$.

Substitution of Eq.(22) into Eq.(21) yields

$$\lambda = G_{11} = [1 + i \cdot \{\rho \cdot B^2 \cdot H^*_1 / (2m) - 2h^s_1\}] / \omega_1^2 \quad \cdots\cdots (21a)$$

The imaginary part of Eq.(21a) must be zero when galloping occurs. Then, the galloping criterion is

$$h^s_1 - \rho \cdot B^2 \cdot H^*_1 / (4m) = 0 \quad \cdots\cdots (23)$$

where h^s_1 is the structural damping for vertical oscillation. When the quasi-steady theory is valid for girder, H^*_1 may be given as

$$H^*_1 = -[(dC_L/d\alpha) + (A/B) \cdot C_D] / K \quad \cdots\cdots (24)$$

Inserting Eq.(24) into Eq.(23), the galloping criterion by the quasi-steady theory is [9), 10)]

$$h^s_1 + \rho \cdot B^2 \cdot [(dC_L/d\alpha) + (A/B) \cdot C_D] / (4m \cdot K) = 0 \quad \cdots\cdots (25)$$

(2) SDOF Torsional Flutter

SDOF torsional flutter is often called stall flutter. Applying the same procedure as the galloping:

$$E_{11} = \rho \cdot B^4 \cdot A^*_2 / (2I) \quad \cdots\cdots (26)$$

$$F_{11} = \rho \cdot B^4 \cdot A^*_3 / (2I) \quad \cdots\cdots (27)$$

where I is the polar moment of inertia per unit length $[t \cdot s^2]$. Inserting Eqs.(26) and (27) into Eq.(21) then setting the imaginary part to be zero, the criteria of SDOF torsional flutter is obtained as follows:

$$\left.\begin{aligned} h^s_1 \cdot \frac{\omega_1}{\omega} - \rho \cdot B^4 \cdot A^*_2 /(4I) = 0 \\ \omega^2 = \omega_1^2 /[1 + \rho \cdot B^4 \cdot A^*_3 /(2I)] \end{aligned}\right\} \quad \cdots\cdots (28)$$

Successive iteration of Eq. (28) for ω and $V = B \cdot \omega_R / K$ gives flutter frequency and velocity, as corresponding to Eqs. (13) – (15) of Ref. 3).

5. 2-DOF COUPLED FLUTTER

2–DOF coupled flutter of spring-mounted section model usually consists of vertical bending and torsional modes. The present theory gives complex eigenvalue equations as follows.

$$\begin{bmatrix} G_{11} - \lambda & G_{12} \\ G_{21} & G_{22} - \lambda \end{bmatrix} \cdot \begin{Bmatrix} X_1 \\ X_2 \end{Bmatrix} = 0 \quad \cdots\cdots (32)$$

$$\begin{vmatrix} G_{11} - \lambda & G_{12} \\ G_{21} & G_{22} - \lambda \end{vmatrix} = 0 \quad \cdots\cdots (33)$$

Then the following complex quadratic equations should be solved to get λ (cf. suffix 1: torsion and suffix 2: vertical bending).

$$\lambda^2 - (G_{11} + G_{22}) \cdot \lambda + G_{11} \cdot G_{22} - G_{12} \cdot G_{21} = 0 \quad \cdots\cdots (34)$$

where

$$\left.\begin{aligned} G_{11} &= (F_{11} + 1)/\omega_1^2 + i \cdot \{E_{11} - 2h^s_1 \cdot \omega_1/\omega\}/\omega_1^2 \\ G_{22} &= (F_{22} + 1)/\omega_2^2 + i \cdot \{E_{22} - 2h^s_2 \cdot \omega_2/\omega\}/\omega_2^2 \\ G_{12} &= (F_{12} + i \cdot E_{12})/\omega_1^2 \\ G_{21} &= (F_{21} + i \cdot E_{21})/\omega_1^2 \\ E_{11} &= \rho \cdot B^4 \cdot A^*_2 /(2I) \\ E_{22} &= \rho \cdot B^2 \cdot H^*_1 /(2m) \\ E_{12} &= \rho \cdot B^3 \cdot A^*_1 /(2I) \\ E_{21} &= \rho \cdot B^3 \cdot H^*_2 /(2m) \\ F_{11} &= \rho \cdot B^4 \cdot A^*_3 /(2I),\ F_{22} = 0,\ F_{12} = 0 \\ F_{21} &= \rho \cdot B^3 \cdot H^*_3 /(2m) \end{aligned}\right\} \quad \cdots\cdots (35)$$

To solve Eq.(34), initial values of $\omega_1/\omega = 1$ or $\omega_2/\omega = 1$ may be adopted. For the successively assumed values of reduced frequency K, one will find the flutter velocity where imaginary part of $\omega = 1/\sqrt{\lambda}$ (i.e., ω_I) is zero. The amplitude ratio $|X_2/X_1| = |(\lambda - G_{11})/G_{12}|$ and phase-shift $\theta = \tan^{-1}(X_2/X_1)$ are also obtained. An example of this application will be shown in chapter 6.

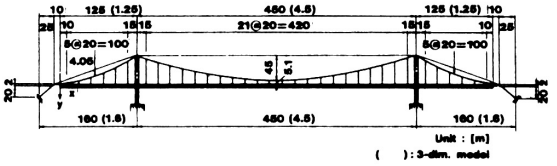

Fig.2 Mono-Cable Suspension Bridge

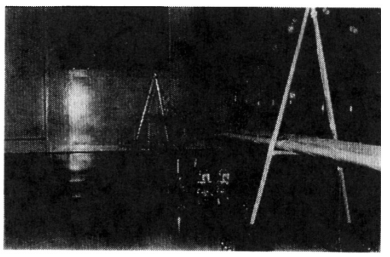

Photo 1 3-Dim. Model

6. ANALYSIS MODEL AND WIND-TUNNEL TEST

A mono-cable suspension bridge (**Fig.2**) with a continuous main girder was selected mainly to examine the non-analogous coupled mode flutter behavior. The effects of higher (i.e., 2nd and 3rd) vertical bending modes are also examined, though they are not so distinctive as the cases in Ref. 11). However, as the bridge model possesses only slight lateral motions in the 1st torsional mode and $dC_D/d\alpha \cdot C_L \cdot C_M$ in Eq. (6) are also insignificant at angle of attack $\alpha = 0°$ and its vicinity, the discussions on the effects of lateral motions[6),7),11)] and their possible coupling with other (i.e., vertical or torsional) motions are abandoned. Thus, in the following analysis, all the flutter derivatives in Eq. (6) are set as (= 0).

(1) Structural Model for Analysis

The mono-cable suspension bridge (**Photo 1**) is idealized as a three dimensional frame-work (**Fig.3**). The girder is supported only laterally at the tower to lessen intermediate support moments. As the result, the frequencies of the first symmetric vertical bending and torsional oscillations become close and the coupled-flutter occurs easily. Using the space-frame model, natural frequencies and mode-shapes were calculated. The equivalent mass and the moment of inertia were applied for the section model tests. Static displacements due to wind loads were also computed to verify the structural similarity of the three-dimensional model.

(2) Section Model

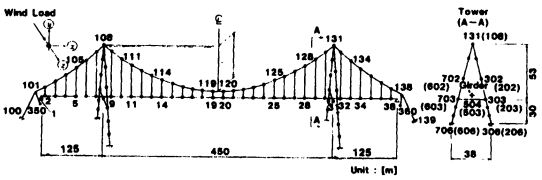

Fig.3 Analysis Model of Mono-Cable Suspension Bridge

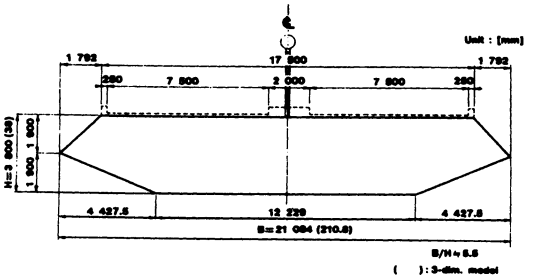

Fig.4 Tapered Box Section

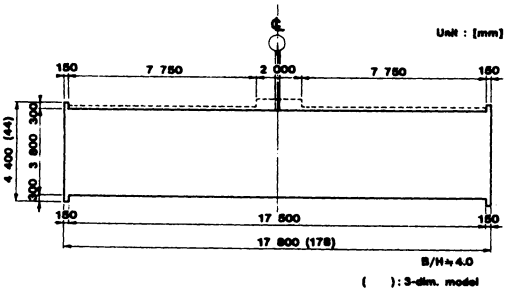

Fig.5 Rectangular Box Section

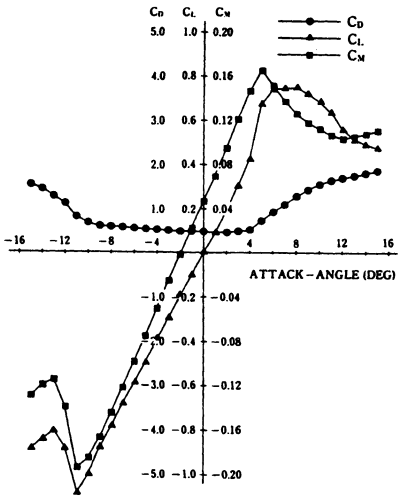

Fig.6 Drag, Lift and Moment Coefficients of Tapered Box Section

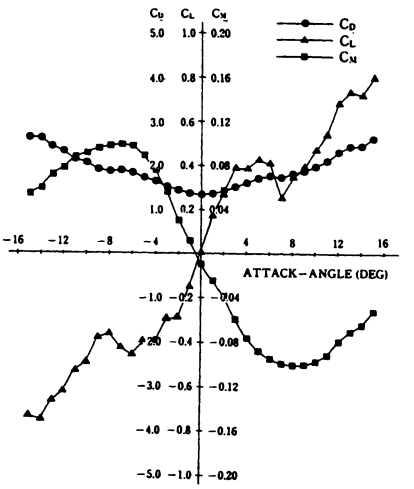

Fig.7 Drag, Lift and Moment Coefficients of Rectangular Box Section

Table 1 Section Model (Tapered Box)

$\alpha = 0°$

Item	Prototype	Required Values		Model
Scale	1	1/n	1/50	1/50
Mass	30.08 t/m	$1/n^2$	12.03 kg/m	11.90 kg/m
Mass Moment	109.24 t·m·s^2/m	$1/n^4$	0.0175 kg·m·s^2/m	0.0174 kg·m·s^2/m
Vertical Freq.	0.2424	$\sqrt{n}$	1.714	1.650 (1.651*)
Torsional Freq.	0.2999	$\sqrt{n}$	2.121	2.122 (2.125*)
Feq. Ratio	1.237	1	1.237	1.286 (1.287*)

N.B.) * denotes $\alpha = 3°$

Table 2 Section Model (Rectangular Box)

$\alpha = 0°$

Item	Prototype	Required Values		Model
Scale	1	1/n	1/50	1/50
Mass	30.08 t/m	$1/n^2$	12.03 kg/m	11.98 kg/m
Mass Moment	109.24 t·m·s^2/m	$1/n^4$	0.0175 kg·m·s^2/m	0.0173 kg·m·s^2/m
Vertical Freq.	0.2424	$\sqrt{n}$	1.714	1.647 (1.649*)
Torsional Freq.	0.2999	$\sqrt{n}$	2.121	2.111 (2.112*)
Feq. Ratio	1.237	1	1.237	1.282 (1.281*)

N.B.) * denotes $\alpha = 3°$

The configuration of the girder was assumed to be either tapered or rectangular box-section (**Figs.4,5**) and 1/50 scale section models were used. Experimental conditions are shown in **Table 1,2**. Drag, lift and moment coefficients measured for these models are shown in **Figs.6** and **7**.

(3) 3-D Model

Three-dimensional model (1/100 scale) is shown in **Photo 1**. The original rectangular box-section was altered to tapered one by adding fairings. Modal shapes

Mode Shape —— Analysis ● Measured on Model	Analysis Prototype f_i [Hz]	Measured Model $\frac{f_i}{\sqrt{100}}$ [Hz]	Model Damping δ_i
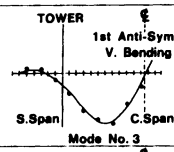	0.2219	0.225	0.079
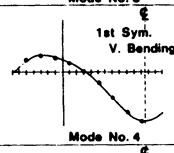	0.2424	0.253	0.014
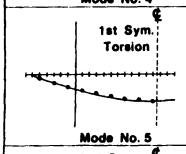	0.2999	0.313	0.012
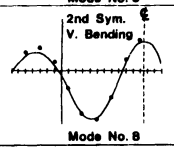	0.3745	0.371	0.014

Fig.8 Frequencies and modes of 3-D model

Table 3 Three-dimensional Model

n = 100

Item	Prototype	Required Values		Model
Scale	1	1/n	1/100	1/100
Mass				
Cable	3.4 t/m	$1/n^2$	3.4 g/cm	3.4 g/cm
Girder	26.5 t/m	$1/n^2$	26.5 g/cm	26.5 g/cm
Tower	14.5 t/m	$1/n^2$	14.5 g/cm	4.8 g/cm
Mass Moment				
Girder	1060 tm^2/m	$1/n^4$	1060 $g\cdot cm^2$/cm	1060 $g\cdot cm^2$/cm
Stiffness				
Girder				
Vertical (EI_z)	4.14×10^7 tfm^2/Br	$1/n^5$	4.14 $kgf\cdot m^2$	4.14 $kgf\cdot m^2$
Lateral (EI_y)	55.1×10^7 tfm^2/Br	$1/n^5$	55.1 $kgf\cdot m^2$	85.9 $kgf\cdot m^2$
Torsion (GJ)	1.67×10^7 tfm^2/Br	$1/n^5$	1.67 $kgf\cdot m^2$	1.67 $kgf\cdot m^2$
Cable (EA)	0.82×10^7 tf	$1/n^3$	8.2×10^3 kgf/Br	5.7×10^3 kgf/Br
Frequency				
Vertical	0.2424 Hz	$\sqrt{n}$	2.424	2.53
Torsion	0.2999 Hz	$\sqrt{n}$	2.999	3.13
Freq. Ratio	1.237	1	1.237	1.237

of the model agreed well with the analytical values (**Fig.8**). The dimensions and properties of both prototype and model are listed in **Table 3**.

(4) Flutter Derivatives

Flutter derivatives $H^*_i(K)\cdot A^*_i(K)$ (i=1,2,3) were measured by the forced vibration method using the section models. Basically the flutter derivatives are dependent on the amplitudes of oscillating body[12),13)] so that they were measured for sinusoidal vertical motions of $y_0 = 5^{mm}\cdot10^{mm}$ (2Hz) and torsional motions of $\alpha_0 = 1°\cdot 2°$ (3Hz)[14)]. As the amplitude-dependency (i.e., non-linearity) of the flutter derivatives were confirmed to be insignificant for the girder sections under review, $H^*_i(K)\cdot A^*_i(K)$(i=1,2,3) measured at the amplitudes of $y_0=10^{mm}$ and $\alpha_0=1°$ have been applied for the following flutter analysis (**Figs.9** and **10**).

7. DISCUSSION OF RESULTS

As the bridge model has no vertical shoes at the towers, the lowest vertical bending (No.4) and torsional (No.5) modes (**Fig.11**) have evidently non-analogous shape along the span. The non-analogous component defined in **Fig.12** tends to increase aerodynamic damping[2)]. Also the non-analogous component of the second and third vertical bending modes (No.6, 8) will have the same effect when their coupling with torsional oscillation (No.5) occurs.

In the present analysis, multi-mode flutter analysis adopting four modes (No.4, 5, 6, 8 in **Fig.11**, i.e., the lowest torsional mode and the lowest three vertical modes), two-mode flutter analysis (No.4, 5) and 2-DOF analysis (see chapter 5) are performed. The first and second analyses are comparable with 3-D model test, while the third analysis corresponds to section model test. V-δ curves by analysis and wind tunnel tests are shown in **Figs.13** and **14**. Corresponding modal amplitude ratios (tapered box section) by multi-mode analysis are plotted in **Fig.15**. The modal coupling is distinctive only in the case of tapered box section (α=0°), and in other cases (i.e., tapered box section: α=3° and rectangular box section), almost pure torsional (or stall) flutter is observed (**Fig.15**).

In **Fig.13**(a), multi-mode analysis and 3-D model test foretell virtually identical flutter velocity of V_{cr} = 61–62 (m/s), while two-mode analysis gives slightly lower critical velocity of V_{cr} = 60 (m/s). The difference is provided by the effect of higher vertical modes (No.6 and 8). 2-DOF analysis and section model test are also in good agreement, but they considerably underestimate the flutter velocity giving V_{cr} = 47–48 (m/s). The disparity is attributable to the aerodynamic damping produced by coupling of non-analogous vertical and torsional modes which is inevitably excluded from 2-

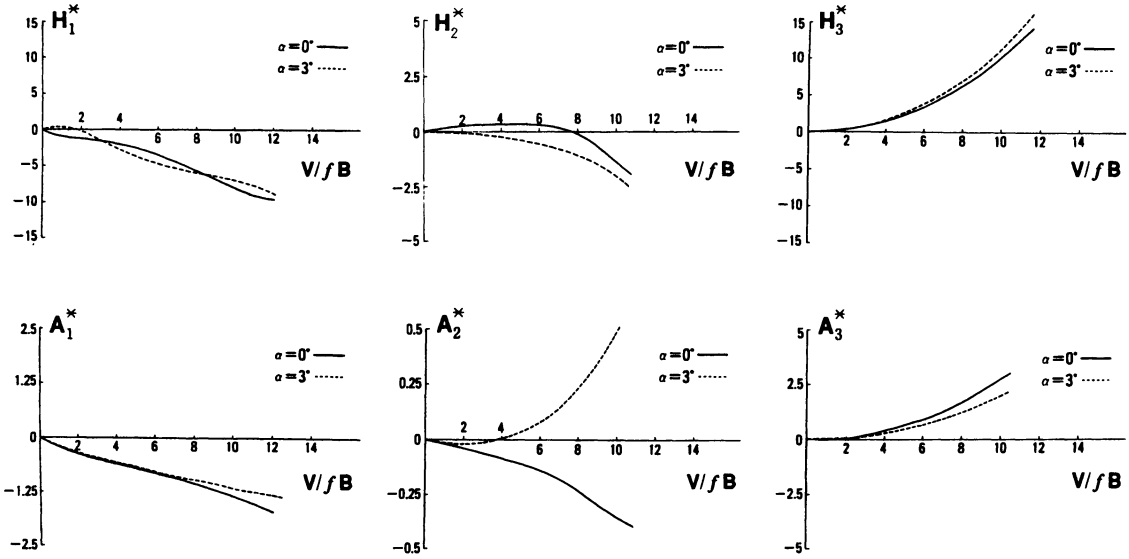

Fig.9 Flutter Derivatives for Tapered Box Section

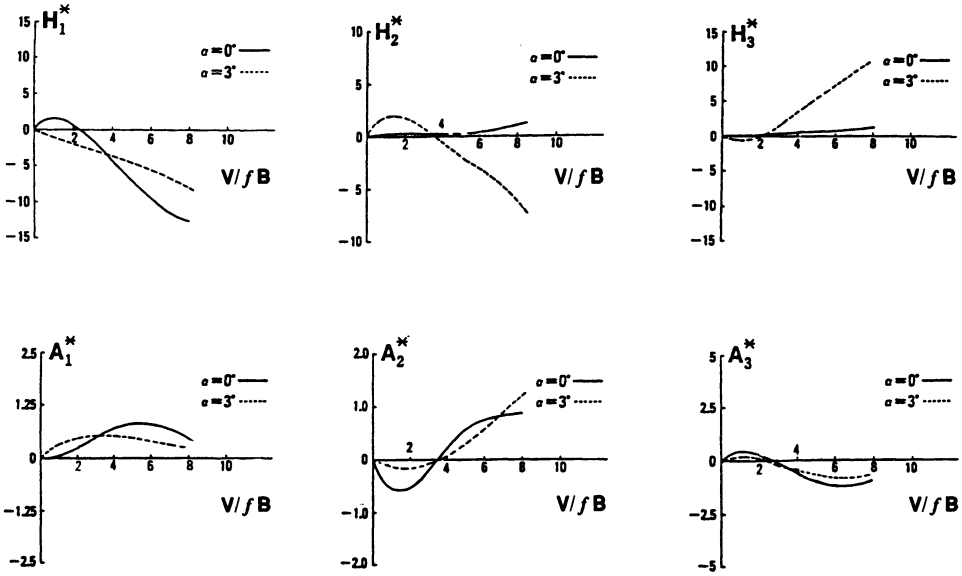

Fig.10 Flutter Derivatives for Rectangular Box Section

DOF analysis and section model test. The details of 2-DOF analysis are shown in **Tables 4** and **5**.

In other cases (**Figs.13**(b), **14**, **15**(b)), where nearly pure torsional (or stall) flutter is evoked, better agreement can be observed among multi-mode analysis, 3-D model test and section model test. Referring to Eq.(28), it is apparent that the pure torsional (or stall) flutter velocity is almost exclusively dependent on the flutter derivative A^*_2, and , as is usually the case with, V_{cr} is found to be a little higher than the wind speed where A^*_2 turns positive.

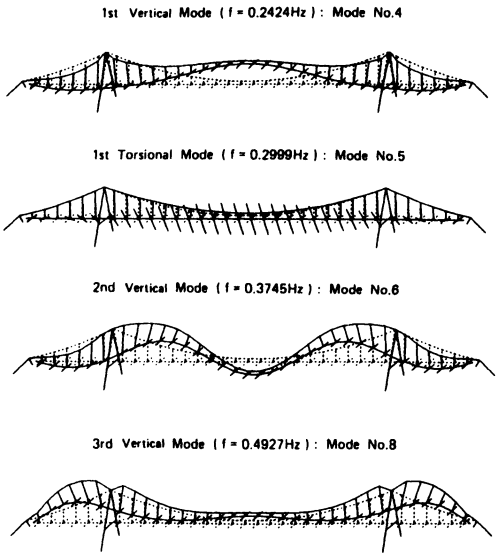

Fig.11 Lowest vibration modes

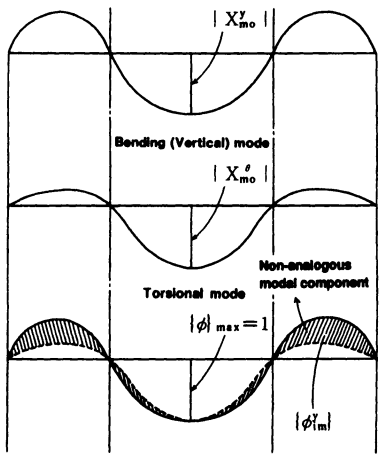

Fig.12 Non-analogous modal component

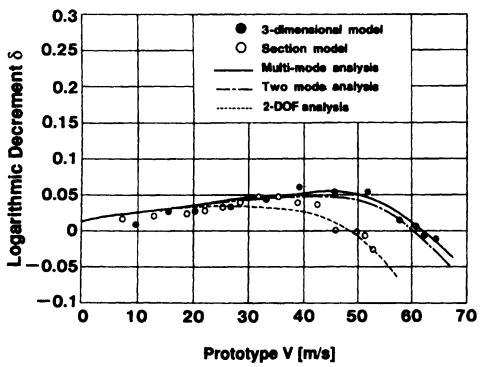

(a) $\alpha = 0°$

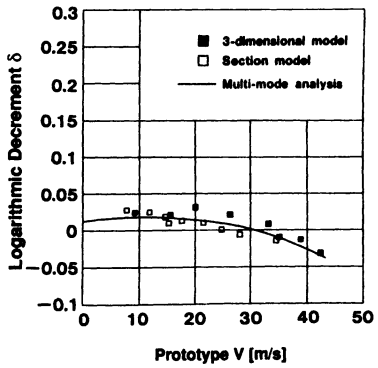

(b) $\alpha = 3°$

Fig.13 V-δ Curves for the Tapered Box Section

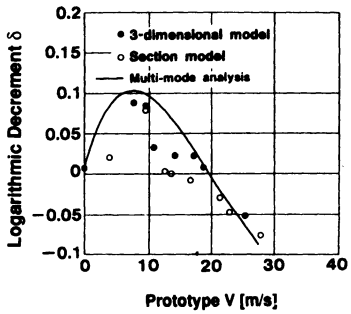

(a) $\alpha = 0°$

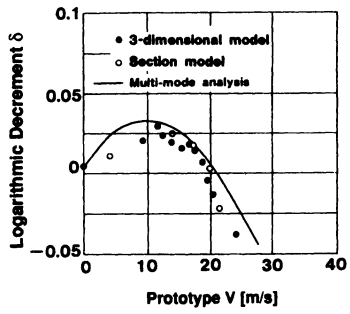

(b) $\alpha = 3°$

Fig.14 V-δ Curves for the Rectangular Box Section

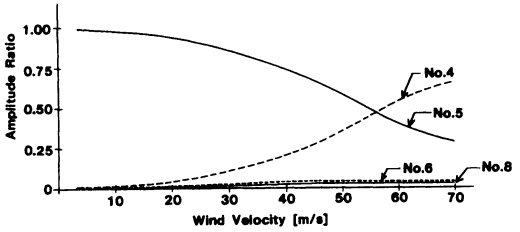

(a) Tapered Box Section ($\alpha = 0°$)

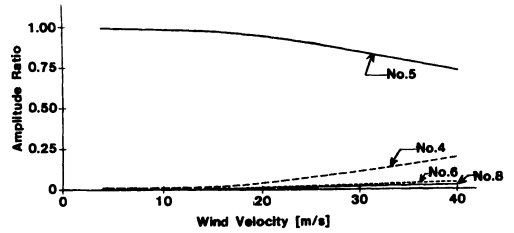

(b) Tapered Box Section ($\alpha = +3°$)

Fig.15 Amplitude Ratio of Multi-Mode Flutter

Table 4 Flutter Derivatives for Tapered Box Section ($\alpha = 0°$)

V/f·B	H^*_1	H^*_2	H^*_3	A^*_1	A^*_2	A^*_3
2.0	−1.234	0.355	0.367	−0.388	−0.053	0.129
3.0	−1.575	0.323	0.773	−0.517	−0.070	0.241
4.0	−2.018	0.309	1.442	−0.627	−0.091	0.416
5.0	−2.662	0.318	2.127	−0.730	−0.111	0.592
6.0	−3.533	0.322	3.060	−0.837	−0.137	0.837
7.0	−4.599	0.238	4.473	−0.953	−0.175	1.224
8.0	−5.788	0.077	5.504	−1.082	−0.230	1.519
9.0	−6.996	−0.458	7.480	−1.226	−0.293	2.095
10.0	−8.110	−1.124	9.298	−1.385	−0.352	2.588
11.0	−9.019	−1.790	11.116	−1.556	−0.401	3.081
12.0	−9.631	−2.800	15.015	−1.738	−0.437	3.888

Table 5 Complex Frequencies of Tapered Box Section ($\alpha = 0°$· 2-DOF Analysis)

V(m/s)	ω_R	ω_I	$\delta = 2\pi \cdot h$ $(h = \omega_I/\omega_R)$
3.5	1.8814	0.0049	0.0164
7.0	1.8784	0.0060	0.0202
10.5	1.8755	0.0071	0.0238
14.0	1.8726	0.0081	0.0273
17.5	1.8664	0.0090	0.0303
21.0	1.8571	0.0095	0.0323
24.5	1.8460	0.0099	0.0336
28.0	1.8334	0.0099	0.0340
31.5	1.8192	0.0096	0.0333
35.0	1.8029	0.0090	0.0312
38.5	1.7849	0.0077	0.0273
42.0	1.7645	0.0058	0.0207
45.5	1.7421	0.0031	0.0112
49.0	1.7179	−0.0052	−0.0191
52.5	1.6934	−0.0063	−0.0233
56.0	1.6702	−0.0139	−0.0523
59.5	1.6516	−0.0222	−0.0843
63.0	1.6353	−0.0310	−0.1190
66.5	1.6191	−0.0396	−0.1538
70.0	1.6028	−0.0481	−0.1885

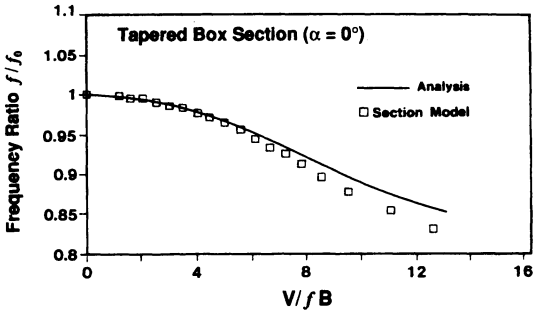

Fig.16 Frequency Ratio f/f_0 of Section Model

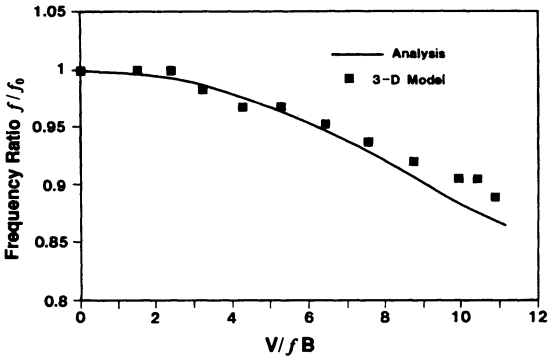

(a) Tapered Box Section ($\alpha = 0°$)

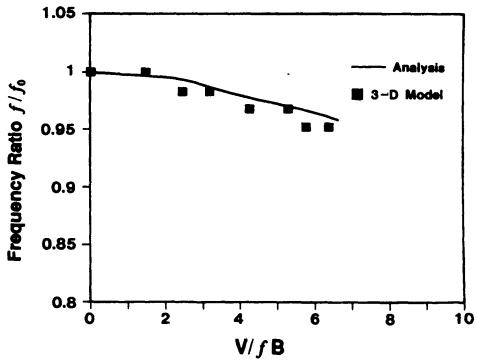

(b) Tapered Box Section ($\alpha = 3°$)

Fig.17 Frequency Ratio f/f_0 of 3-D Model and Multi-mode Analysis

In the following discussions, the cases are narrowed down to tapered box section with multi-mode coupling motions. First, the ratios of flutter frequencies to torsional frequency f_0 in still air are plotted in **Figs.16** and **17**. It decreases rather swiftly with the increase of wind speed and is appropriately predicted by the present analysis for both section model and 3-D model. The decrease is attributable to the effect of aerodynamic terms $P^*_3 \cdot H^*_3 \cdot A^*_3$, and naturally, the flutter frequency of 3-D model (**Fig.17**) decreases more rapidly in the case of $\alpha = 0°$ as against $\alpha = 3°$ because of larger coupling motions.

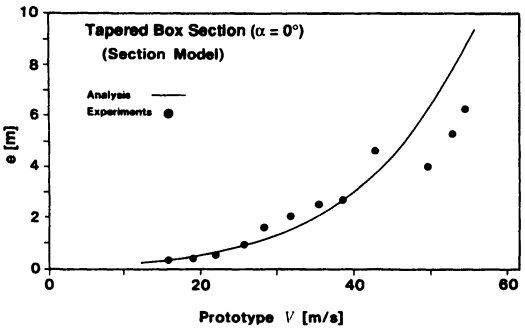

Fig.18 Shift of Rotational Center e[m] (Section Model)

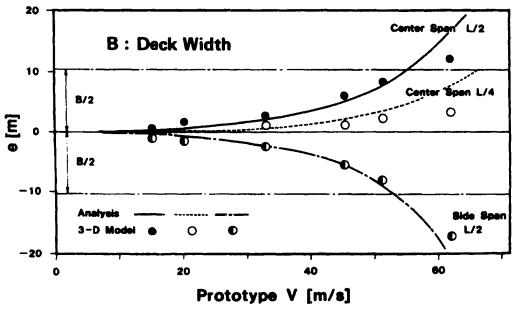

(a) Tapered Box Section (α = 0°)

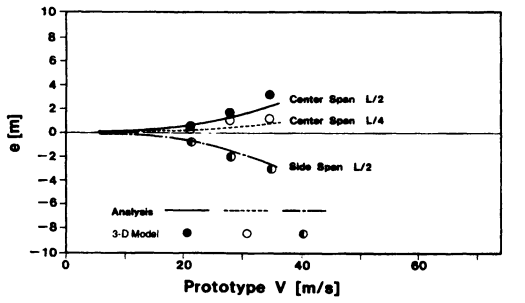

(b) Tapered Box Section (α = 3°)

Fig.19 Shift of Rotational Center e[m] (3-D Model and Multi-mode Analysis)

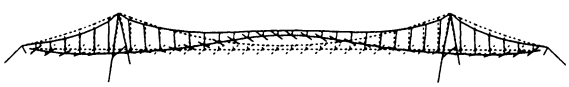

Fig.20 Flutter Mode of Tapered Box Section (α = 0°, V = 62 m/s) by Multi-mode Analysis

As for the shift (i.e., lateral locations) of rotational center, analytical results are almost identical with the experimental ones (**Figs.18, 19**). Note that if a coupled flutter involves only analogous modes (e.g., in the case of a simple beam[6),7),8)]), then $X_y \cdot \phi^y(x)/X_\alpha \cdot \phi^\alpha(x)$ (y: vertical and α: torsional) is exclusively dependent on the wind velocity and the lateral locations of rotational center do not vary along the span. However, in this case, it is shown that the lateral locations of rotational center of 3-D model vary evidently along the span (**Figs.19, 20**) mainly due to the coupling of non-analogous vertical and torsional modes (No.4 and No.5). If the amplitude ratios of higher modes are large, they also contribute to the shift of rotational center. Then, it is concluded that section model can not represent the prototype bridge behavior so far as the coupled non-analogous and/or multi-mode flutter is discussed.

8. CONCLUSIONS

If a coupled flutter is associated with non-analogous and/or the higher modes, the present analysis using the flutter derivatives seems to be useful along with the three-dimensional model tests. The analysis can reflect the change of aerodynamic properties of the girder (including the flutter derivatives) along the span, and additional damping effects provided by the lateral motions of girder and by the motions of cables and towers. The authors also proposed a quasi-steady formulation of $P^*_0 \cdot H^*_0 \cdot A^*_0$, though tentatively defined (i.e., yet to be proved), to include possible coupling between lateral and other (vertical or torsional) motions of girder. In the cases discussed in this paper, the section model tests can not be regarded as representative of the prototype bridge action and they may instead serve as the source of aerodynamic data such as the flutter derivatives.

ACKNOWLEDGEMENT

The authors extend sincere appreciation to Dr. Toshio UEDA, Mr. Hiroyuki SUNADA and Mr. Eiji YAMAGUCHI, Hitachi Zosen Corp., for their assistance of wind tunnel tests.

REFERENCES

1) Farquharson, F.B., ed.: Aerodynamic Stability of Suspension Bridges, The Structural Research Laboratory at University of Washington, Part I-V, June 1949 - June 1954.

2) Bleich, F.: Dynamic Instability of Truss-Stiffened Suspension Bridges under Wind Action, Trans. ASCE, Vol.114, pp.1177-1232, 1949.

3) Scanlan, R.H.: The Action of Flexible Bridges under Wind, Part I (Flutter Theory), Journal of Sound and Vibration, 60(2), pp.187-199, 1978.

4) Miyata, T. Yamada, H. and Ohta, H.: Flutter Analysis of a Truss Stiffening Suspension Bridge by 3D Model Method, Proc. of JSCE, Vol.404, pp.267-275, April 1989 (in Japanese).

5) Scanlan, R.H.: Interpreting Aeroelastic Models of Cable-Stayed Bridges, Journal of Engineering Mechanics, ASCE, Vol.113, No.EM4, pp.555-575, April 1987.

6) Yamamura N., Tanaka, H. and Ueda T.: 2-DOF Aerodynamic Modeling for 3-Dimensional Flutter Behavior of Long-Span Bridges (2nd Report), Hitachi Zosen Technical Review, Vol.51, No.1, June 1990, pp.30-48 (in Japanese).

7) Tanaka, H., Yamamura N. and Tatsumi, M.: Coupling Mode Flutter Analysis Using Flutter Derivatives, Eighth International Conf. on Wind Eng., Journal of Wind Eng. and Ind. Aerodynamics, 41-44, pp.1279-1290, 1992.

8) Tanaka, H. and Yamamura, N.: Coupled Flutter Analysis for Flexible Long-span Bridges with Flutter Derivatives, Proc. of 11th National Symposium on Wind Eng., Dec. 1990 (in Japanese).

9) Den Hartog. J.P.: Mechanical Vibrations, Dover Publications, Inc., New York, 1985.

10) Simiu, E. and Scanlan, R.H.: Wind Effects on Structures, Wiley, New York, 1978.

11) Yasuda, M., Kanasaki, T., Katsuchi, H., Ueda, T., Tanaka, H. and Hikami, Y.: Aerodynamic Stability of a Long-Span Suspension Bridge by Flutter Analysis & Wind Tunnel Tests, Proc. of 12th National Symposium on Wind Eng. Dec. 1992 (in Japanese).

12) Shiraishi, N. and Ogawa, K.: An Investigation on Aeroelastic Response of Suspension Bridges due to the Non-Linear Aerodynamic Forces, Proc. of JSCE, No.244, pp.23-35, 1975.

13) Kubo, Y., Ito, M. and Miyata, T.: Nonlinear Analysis of Aerodynamic Response of Suspension Bridges in Wind, Proc. of JSCE, No.252, pp.35-46, 1976.

14) Tanaka, H.: Aerodynamic Stability of Long Span Bridges due to Unsteady Aerodynamic Forces, Doctor Dissertation, Kyoto Univ., Jan. 1993.

(Received November 17, 1992)

非相似なモード形状を有する橋梁に関する多重モードフラッター解析と２次元及び３次元風洞実験

田中　洋・山村信道・白石成人

長大橋梁における連成フラッターは，従来，曲げ（鉛直）・ねじれの２自由度で議論されることが多かったが，非相似なモード形状を有する橋梁に対しては，モード形状を考慮したモーダル・アナリシスを行う必要がある．本論文は，橋体の橋軸直角（水平）方向変位も加えた多重モード解析の定式化とモノケーブル吊橋（梯形・矩形断面の２種類）を用いた２次元，及び，３次元の風洞実験を行い，フラッター風速・V-δ曲線・振動数変化・振幅比・回転中心の移動等に着目して，理論と実験結果の比較・考察を行った．